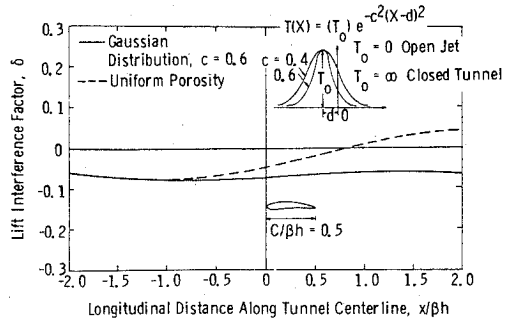

Fig. 2 Lift interference for NASA 64-series airfoil in tunnels with Gaussian and uniform distributions of porosities at $\beta T(x=0)=4.0$, $d/\beta h=-1.0$.

The results of lift interference for the NACA-64 airfoil series in tunnel walls with Gaussian and uniform distribution of porosities are shown in Fig. 2. The comparison between these two curves indicates that improvement of lift interference is found by utilizing the Gaussian distribution. Specifically, the lift interference at the tail has the same sign and magnitude as that at the wing for a wing-tail model.

The pitching moment obtained from a uniform distributed porosity tunnel which has opposite signs of interference between the wing and the tail is difficult to correct. In a Gaussian distribution of porosity, the interference has the same sign and magnitude on the wing and the tail. The only correction required to the model data is for tunnel flow angularity.

Blockage Interference

For the blockage interference calculation, the model potential for the airfoil thickness is represented by

$$\phi_m = \frac{U_\infty}{\pi}\int_o^{C_h}\frac{dy_t(\zeta)}{dx}\log\left[(x-\zeta)^2+y^2\right]^{1/2}d\zeta$$

Similarly to the lift interference case, a discrete distribution of source singularities is adopted as

$$\phi_m = \sum_j \Delta\phi_{m,j}$$

$$= \frac{U_\infty}{\pi}\sum_j \frac{dy_t(\zeta_j)}{dx}\Delta\zeta_j\cdot\log\left[(x-\zeta_j)^2+y^2\right]^{1/2}$$

The formulation is set up for each single discrete model potential in terms of the axial perturbation velocity.

The blockage interference, $\epsilon=u_i/\beta hU$, is calculated[8] for a biconvex airfoil shown in Fig. 3 for $C_h=0.3$ and 0.5. The comparison demonstrates clearly that the blockage interference gradient for uniform porosity is greatly reduced by using the Gaussian distribution. In the uniform porosity tunnel, the blockage interference not only has a rather large gradient but also changes signs from the leading edge to the trailing edge of airfoil.

Conclusions

The solution is computationally simplified by assuming a discrete distribution of singularities for a finite chord airfoil. The form of influence coefficients is obtained for a given wind tunnel. The tabulated influence coefficients can be used to calculate interference factors for any finite airfoil with a given loading and thickness distribution at a given angle of attack.

The potential to reduce tunnel interferences on a given finite airfoil is demonstrated by a selected Gaussian distribution of porosity. For a specific airfoil, one of a family of Gaussian distribution may be used for interference minimization although superior porosity distributions may be found for the general case.

The interference calculation for the previous examples indicates that a large gradient of porosity, especially in the neighborhood of the test model, is required to significantly

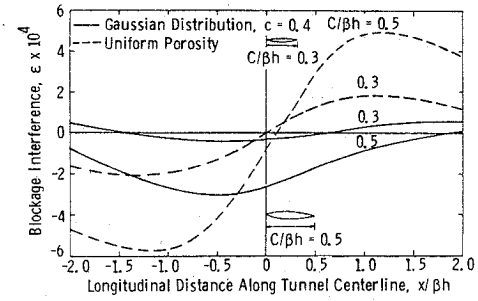

Fig. 3 Blockage interference for a biconvex airfoil with 6% thickness ratio in tunnels with Gaussian and uniform distributions of porosities at $\beta T(x=o)=1.5$, $d/\beta h=-1.0$.

change the value of interference factors of a tunnel. In other words, any small amount of variation of porosity does not greatly affect tunnel interferences. For the subsonic case, the blockage interference is usually negligible[9] as compared to the lift interference. Hence, the consideration of lift interference should be emphasized in the selection of tunnel wall porosity distribution.

References

[1] Lo, C. F. and Oliver, R. H., "Subsonic Lift Interference in a Wind Tunnel with Perforated Walls," *Journal of Aircraft*, Vol. 7, May-June 1970, pp. 281-283.

[2] Jacocks, J. L., "Evaluation of Interference Effects on a Lifting Model in the AEDC PWT 4-ft Transonic Tunnel," AEDC-TR-70-72 (AD868290), April 1970, Arnold Engineering Development Center, Arnold Air Force Station, Tullahoma, Tenn.

[3] Binion, T. W., Jr., "An Investigation of Several Slotted Wind Tunnel Wall Configurations with a High Disc Loading V/STOL Model," AEDC-TR-71-77 (AD723294), May 1971, Arnold Engineering Development Center, Arnold Air Force Station, Tullahoma, Tenn.

[4] Lo, C. F., "Wind Tunnel Wall Interference Reduction by Streamwise Porosity Distribution," *AIAA Journal*, Vol. 10, April 1972, pp. 547-550.

[5] Sears, W. R., "Self-Correcting Wind Tunnels," Rept. RK-5070-A-2, July 1973, Calspan Corp., Buffalo, N.Y.

[6] Baronti, P., Ferri, A., and Weeks, T., "Analysis of Wall Modification in a Transonic Wall Tunnel," Rept. TR-181, Feb. 1973, Advanced Technology Labs, Westbury, N.Y.

[7] Erickson, J.C. Jr., and Nerni, J. P., "A Numerical Demonstration of the Establishment of Unconfined-Flow Conditions in a Self-Correcting Wind Tunnel," Rept. RK-5070-A-1, Nov. 1973, Calspan Corp., Buffalo, N.Y.

[8] Ladd, T. G., "Lift Interference Factor and Blockage Factors in Some Perforated Wind Tunnels," Ms thesis, Dec. 1972, Dept. of Mathematics, University of Tennessee, Knoxville, Tenn.

[9] Pindzola, M. and Lo, C. F., "Boundary Interference at Subsonic Speeds in Wind Tunnels with Ventilated Walls," AEDC-TR-69-47, May 1969, Arnold Engineering Development Center, Arnold Air Force Station, Tullahoma, Tenn.

Effect of Combined Roll Rate and Sideslip Angle on Aircraft Flight Stability

Robert F. Stengel*
The Analytic Sciences Corporation, Reading, Mass.

Introduction

IT has long been known that rapid roll rates can destabilize the motions of aircraft. The introduction of high-

Received December 2, 1974. This research was conducted at The Charles Stark Draper Laboratory under NASA Contract NAS9-10268.

Index categories: Aircraft Handling, Stability, and Control; Navigation, Control, and Guidance Theory; Spacecraft Attitude Dynamics and Control.

*Member of the Technical Staff. Associate Fellow AIAA.

performance aircraft following World War II demonstrated the problem, motivating the classic analysis of Phillips in 1948.[1] This analysis has been extended, as reported in Refs. 2-4, with primary attention paid to the case of zero sideslip angle. In such an instance, the resonance between longitudinal and lateral-directional motion is coupled by roll rates of the same order as the natural frequencies of the short period and Dutch roll modes. Effects of coupling induced by sideslip with zero angular rates are reported in Refs. 5 and 6, which indicate that sideslip alone is only mildly destabilizing; however, nonzero sideslip angle can lead to adverse coupling at much lower roll rates than would be predicted by roll resonance alone.

These combined destabilizing effects of roll rate and sideslip angle have been examined using a linear simulation of the coupled motions of a Space Shuttle-like configuration. Variations in the eigenvalues for a flight condition nominally identified by angle of attack (α) = 33.29° and Mach number (M) = 4.9 are examined with illustrations of the separate effects of body-axis roll rate (p_B) and yaw rate (r_B), stability-axis roll rate (p_S), dynamic pressure (q), and sideslip angle (β).

Numerical Results

The combined differential equations of the longitudinal and lateral-directional motions of the vehicle are 12th order, with state variables representing angular orientation and rates, as well as translational position and velocity. The eigenvalues of the longitudinal and lateral-directional modes are coupled if the reference values of roll rate, yaw rate, pitch rate, or sideslip angle are nonzero. All 12 eigenvalues have been computed for a flight condition representing the Space Shuttle's return from orbit, although attention will be directed to the short period and Dutch roll complex pairs. As a result of steep entry angle, the phugoid mode has degenerated into two real eigenvalues, representing a velocity mode and a flight path mode in the case considered here. The roll and spiral roots have coalesced in a stable "lateral phugoid" mode, with eigenvalues whose real and imaginary parts are -0.008 and ± 0.007, respectively. The height, range, cross-range, and yaw attitude modes are essentially pure integrations of translational and angular rates. The attitude and velocity are nominally 144,700 ft and 5305 fps, leading to q = 62 psf and M = 4.9 (based on the 1962 U.S. Standard Atmosphere). This leads to the following short period and Dutch roll eigenvalues: short period: (-0.009385, ± 0.6289) (real and imaginary parts); Dutch roll: (-0.008078, ± 0.9887) (real and imaginary parts). Both modes are seen to be lightly damped, and the lateral-directional mode is nearly 60% faster than the longitudinal mode.

Separate Effects of Body-Axis Roll and Yaw Rates

Angular rotation about the body roll axis alone or about the body-yaw-axis alone would lead to nontrivial changes in α and β; hence, linear modeling of a steady rate about either axis is restricted. It is interesting, nevertheless, to examine the progression of the short period and Dutch roll roots for these two cases.

Table 1 presents the effects of body-axis roll rates between 0 and 32 deg/sec. The reference value of β is 0°. It can be seen that the principal effect of body-axis roll rate is to decrease the damping and increase the natural frequencies of both modes; however, neither mode is driven to instability, as the real parts of both modes remain negative.

The effect of body-axis yaw rate is presented in Table 2. There is a similar effect on the Dutch roll natural frequency, but this mode's damping is increased. The short period mode's frequency is relatively unaffected, but its damping becomes negative at a yaw rate of 29 deg/sec, i.e., the root's real part becomes positive.

Effect of Stability-Axis Roll Rate

If the vehicle is rolled about the velocity vector with zero β, the body centerline describes a cone with half-angle equal to α, and the angular rate is transformed into body-axis roll and yaw rates as

$$p_B = p_S \cos\alpha \tag{1}$$

$$r_B = p_S \sin\alpha \tag{2}$$

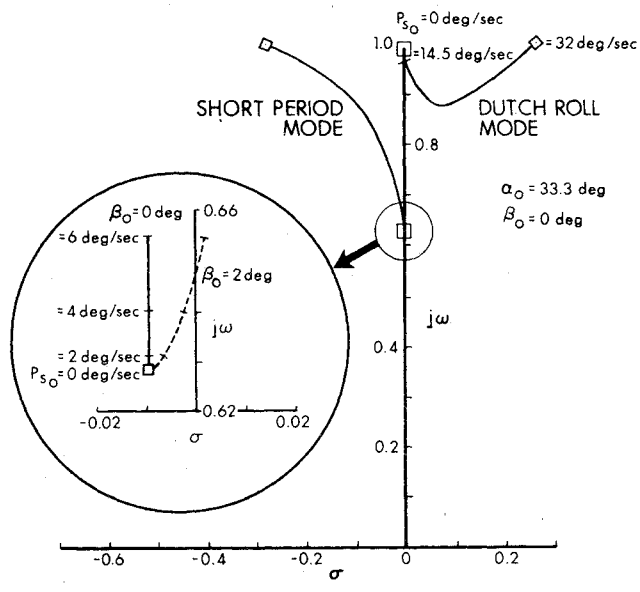

Fig. 1 Example of inertial coupling effects on aircraft dynamic stability.

Table 1 Effect of body-axis roll rate on the roots of the short period and Dutch roll modes

Body-axis roll rate, deg/sec	Short period eigenvalues, rad/sec	Dutch roll eigenvalues, rad/sec
0	-0.009385, ± 0.6287	-0.008078, ± 0.9887
4	-0.009502, ± 0.6300	-0.008077, ± 0.9922
16	-0.009351, ± 0.6507	-0.007970, $\pm$ 1.042
32	-0.009169, ± 0.7271	-0.007734, ± 1.178

Table 2 Effect of body-axis yaw rate on the roots of the short period and dutch roll modes

Body-axis yaw rate, deg/sec	Short period eigenvalues, rad/sec	Dutch roll eigenvalues, rad/sec
0	-0.009385, ± 0.6287	-0.00878, ± 0.9887
4	-0.009186, ± 0.6280	-0.008136, ± 0.9921
16	-0.005666, ± 0.6223	-0.009244, ± 1.043
32	$+0.000928$, ± 0.6201	-0.01041, ± 1.183

Table 3 Effect of sideslip angle on the roots of the short period and Dutch roll modes, $p_S = 0°$

Sideslip angle, deg	Short period eigenvalues, rad/sec	Dutch roll eigenvalues, rad/sec
0	-0.009385, ± 0.6287	-0.008078, ± 0.9887
2	-0.009385, ± 0.6287	-0.008075, ± 0.9886
4	-0.009385, ± 0.6287	-0.008068, ± 0.9883

This motion is realizable, although the gravitational effect on the motion is a function of the roll angle, ϕ. Roll orientation effects are important in the determination of the long period modes but do not affect the attitude modes appreciably. In the current case, with $\cos \alpha = 0.836$ and $\sin \alpha = 0.549$, stability-axis roll rate has the effect shown in Fig. 1. Increasing roll rate stabilizes the short period mode and destabilizes the Dutch roll mode; the latter becomes unstable at a roll rate of 14.5 deg/sec. These results assume no control-loop closures. Augmented damping would materially alter these numerical results, although the trend toward decreased stability with increasing roll rate still would occur.

Effect of Dynamic Pressure

Maintaining velocity magnitude while varying altitude causes significant changes in q and minor changes in M. Some effects of a $\pm 20{,}000$-ft altitude shift are considered here. Reducing the altitude by 20,000 ft increases q to 148 psf, and it increases the stability of the short period and Dutch roll modes. The roll rate at which instability occurs is about 17 deg/sec. Conversely, stability is reduced with increasing altitude. With a 20,000-ft increase, q is reduced to 27 psf, and the Dutch roll mode is slightly unstable, even with zero roll rate (the roots are located at ± 0.0007506, ± 0.6568). Increasing the altitude by 10,000 ft results in $q = 40$ psf. The Dutch roll is stable at this point (with zero roll rate), but it becomes unstable when $p_S = 8$ deg/sec. It is concluded that the stability-axis roll rate at which instability first appears increases as q increases.

Effect of Sideslip Angle

As shown by Table 3, the direct effect of nonzero sideslip angle on the eigenvalues is not large; however, nonzero β causes instability to occur at very low roll rates. The enlarged circle in Fig. 1 illustrates the effect of a β of 2° on the progression of the roots with stability-axis roll rate. The crossover to instability occurs when $p_S = 5$ deg/sec. An interesting result is that the short period mode, not the Dutch roll mode, becomes unstable as a result of the roll rate. Further examination indicates that the short period mode is destabilized when p_S and β have the same sign, but the Dutch roll mode is destabilized when p_S and β have opposite sign. There are insufficient data to indicate whether or not this is a general result; however, it is reasonable to expect differing behavior when the vehicle is side-slipped "into" or "out-of" the rolling motion. Decreasing β to 1° increases the crossover p_S to 10 deg/sec, while increasing β to 4° decreases the roll rate for instability to 3 deg/sec.

Conclusions

The effects of sideslip angle and angular rates have been demonstrated for a high-α flight condition using fully coupled linear equations of motion. It is shown that the stability of the free motion of the vehicle is sensitive to roll rate and that this sensitivity is magnified by nonzero sideslip angle. These results suggest that fully coupled linearized equations can be of value not only for the study of Space Shuttle stability and control, but for a better understanding of post-stall gyrations, incipient spin, and departure prevention for high-performance aircraft.

References

[1] Phillips, W.H., "Effect of Steady Rolling on Longitudinal and Directional Stability," TN 1627, June 1948, NACA.

[2] Abzug, M.J., "Effects of Certain Steady Motions on Small-Disturbance Airplane Motions," *Journal of the Aeronautical Sciences*, Vol. 21, Nov. 1954, pp. 749-762.

[3] Byushgens, G.S. and Studnev, R.V., "Dynamics of the Spatial Motion of an Aircraft," TT F-555, April 1969, NASA.

[4] Etkin, B., *Dynamics of Atmospheric Flight*, Wiley, New York, 1972.

[5] Porter, R.F. and Loomis, J.P., "Examination of an Aerodynamic Coupling Phenomenon," *Journal of Aircraft*, Vol. 2, Nov.-Dec. 1965, pp. 553-556.

[6] Johnston, D.E. and Hogge, J.R., "The Effect of Non-Symmetric Flight on Aircraft High Angle of Attack Handling Qualities and Departure Characteristics," AIAA Paper 74-792, New York, Aug. 1974.

Slide-Valve-Controlled Vectoring Nozzle

J. A. C. Kentfield*
University of Calgary, Calgary, Alberta, Canada

Introduction

SOME time ago, a brief description was given of a ventral-type vectoring nozzle with the flow through the ventral aperture, cut in the wall of the jet pipe, controlled by a slide-valve of curved cross-section conforming to that of the jet pipe.[1] More recently, ventral nozzles with slide-valve control of the ventral orifice were described in further detail.[2] The prime advantages of slide-valve control of the ventral flow are a minimal increment in engine cross-sectional area, compared with that of a nonvectoring engine and simplicity; there is only one major moving part, the slide-valve, associated with the ventral orifice. The advantages of ventral as distinct from other types of vectoring nozzle have been discussed, in relation to a particular mission study, by Gill.[3] The ventral-type vectoring nozzle with slide-valve control appears to be suitable only for engines which are not augmented in the lift mode. Lift mode augmentation creates severe cooling problems with the slide-valve and flow guide-vanes.

This Note presents recently obtained experimental data relating to the aerodynamic performance, including the vectoring capability, of a slide-valve-controlled ventral outflow system. A major factor complicating the design of all ventral vectoring nozzles is the need to provide vector control with the entire engine flow passing through the ventral opening.

Thrust Vector Control

It is particularly important, with ventral nozzles, to arrange for a measure of thrust vector control in the lift mode with the full engine flow passing through the ventral aperture. Vector control, in an elementary ventral nozzle, solely by differential variation of the aft and ventral exit areas, results, due to the geometry of such an arrangement, in a fundamental thrust reduction. With the axes of the two flows at right angles, this reduction has a maximum value of just under 30% when the flow deflection angle θ is 45°; for $\theta = 0°$ and $\theta = 90°$ the reduction is zero. These points are apparent from Fig. 1 from comparison of the curves for the elementary and ideal cases. Figure 1 was established from simple resolution of the thrust forces resulting from outflow through the propulsion and ventral apertures of hypothetical ventral vectoring nozzles.

Full vector control over the range $60° \leqslant \theta \leqslant 90°$ with the entire engine flow passing through the ventral orifice, with the initial flow at 45° when the slide valve begins to open, is suf-

Received February 3, 1975; revision received February 28, 1975.

Index categories: VTOL Aircraft Design; VTOL Missions and Transportation Systems; VTOL Powerplant Design and Installation.

*Associate Professor, Mechanical Engineering Department. Member AIAA.